Numerical simulations and 2D-imaging experiments of flow in tilted crossbeds

Knut Arne Børresen and Arne Graue, University of Bergen

Abstract

Multiphase flow in a heterogeneous reservoir model, 30 *cm* x 10 *cm* x 3 *cm* in size, with moderate variation in petrophysical properties has been studied. The physical model, a sand pack consisting of a high permeable sand with a low permeable sand cutting through the central part of the model at 30° dip angle, represents a tilted crossbedded reservoir. Displacement experiments at low injection rates were performed, and local in-situ saturation development was recorded using a nuclear tracer imaging technique. The influence of the crosslayer was determined for two dip angles, 30° and 150° with respect to the direction of flow, by reversing the flow direction. It was found that the low permeable, high capillary, crossbed dominated the local saturation development. During waterfloods the brine saturation in the central crossbed rapidly increased, due to significant contribution from spontaneous capillary imbibition, when contacted by the waterfront. During this imbibition the inlet- and outlet sands exhibited stagnant oil saturation, reflecting a temporary oil trapping. However, the endpoint saturations eventually reached residual values uniformly distributed within each sand. Hence, permanent oil trapping did not occur in these experiments.

Simulations gave only a qualitatively correct description of the saturation development at a local scale. The results emphasised the importance of knowing the local in-situ saturation development when comparing numerical results with experiments. Numerical simulations predicted less influence on saturation development from the heterogeneities than experimentally observed. Simulations indicated that numerical diffusion induces an unrealistic high waterfront velocity and hence perturbed the local saturation development. Sensitivity analysis showed that grid resolution and relative permeability data was of minor importance, due to dominating capillary forces.

Introduction

The literature reflects an increasing interest for research on reservoir heterogeneities owing to recent increased computational capabilities; making it possible to take advantage of more detailed reservoir descriptions. The detailed reservoir information is obtained at a large scale from improved 3D high resolution seismic data, at macro scale from improved well logging and geological characterisation of core data, and at a micro scale from enhanced laboratory techniques on special core analysis, including micro scale imaging.

In many clastic reservoirs bedded structures are frequently encountered heterogeneities. At *mm* to *m* scale cross-beddings are ubiquitous in fluvial, eolian, and marine deposits (Hartkamp-Baker, 1993). Variation in transport energy during deposition, e.g. changes in water or wind velocity, is the main factor determining texture and bed sequence. Studies of the impacts on oil recovery from beds oriented perpendicular or parallel to flow direction, as the extreme cases of bedded structures, are most frequently reported in the literature (Honarpour *et al.*, 1995; Graue 1990; Sorbie *et al.* 1987; Laribi *et al.* 1995). The heterogeneities are related to variation in permeability and capillarity between internally homogeneous beds.

With respect to a layered structure with brine injection parallel to the bedding, consider a system consisting of a central high permeable layer and two adjacent low permeable layers (Bertin and Quintard, 1990). Assume further that the capillary force is negligible. The front in the high permeable layer is the most advanced and a pressure difference exists between this layer with the most advanced front and the adjacent layers; this pressure difference creates a transverse flow, viscous crossflow. The crossflow pattern depends on the mobility ratio, and is different as the mobility ratio changes from unfavourable to favourable (Wright *et al.*, 1983). In capillary influenced displacements the capillary forces stabilise the front by striving toward equal capillary pressure in all parts of the layered porous media (Ahmed, 1988). If the capillary forces totally dominates the process, the

recovery is driven by surface film flow and the low permeable media is the first to be imbibed. After sufficient brine injected in a layered system residual oil saturation is eventually reached, corresponding to the petrophysical characteristics of each layer.

The other extreme case, heterogeneous systems with bedding perpendicular to flow, shows oil trapping as a characteristic feature. Trapping occurs at the boundary from low to high capillary media (Chaouche *et al.*, 1994; Chang *et al.*, 1993; Graue, 1990). The low permeable medium is quickly imbibed and attain a high water saturation earlier than the high permeable medium upstream. As the low permeable medium downstream reaches a low residual oil saturation, the oil upstream may be trapped due to roughly zero relative permeability downstream (Ringrose *et al.*, 1993; McDougall *et al.*, 1993).

Previous papers are mainly concerned with heterogeneous systems with large contrasts in permeability, porosity and capillary pressure. This paper reports on waterflooding a large scale 2D sandpack model with a less permeable crosslayer at 30° dip angle and moderate variation in the petrophysical parameters. The reservoir model exhibited no porosity contrast, high permeabilities, and about unity fluid mobility ratio. The waterfloods were performed at low rate, thus reflecting a capillary influenced regime. Using a nuclear tracer imaging technique the 2D in-situ brine saturation was monitored. A few studies have previously reported on experiments using large scale two dimensional saturation imaging (Bertin, 1994; Graue, 1995).

A commercial full field simulator, ECLIPSE (Intera), was used to simulate the laboratory experiments.

Material and Methods

A sandpack was prepared in an aluminium container, 30 *cm* x 10 *cm* x 3 *cm* in size, using sand sieved to different grain sizes, see Figure 1, in the following way: coarse sand, consisting of sand grains in the range of 125-250 μm, was used at the injection and production ends, while finer sand, with grains in the range of 60-125 μm, constituted the central section of the cross bedded reservoir model. The tilt angle of the cross bedding relative to flow was 30°.

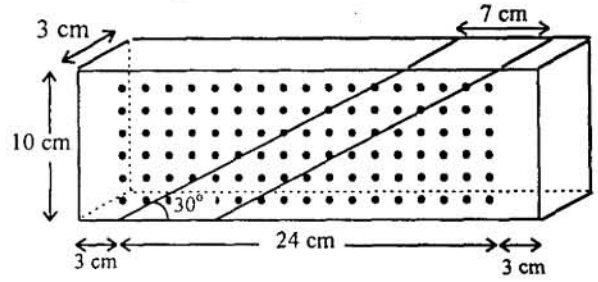

Figure 1 *The heterogeneous reservoir model with the crosslayer indicated. Black dots represent points for in-situ saturation measurements.*

The coarse- and fine sands are earlier reported to have a permeability of 5.7 μm^2 and 3 μm^2 respectively, when using a careful packing procedure (Graue, 1990). The drainage capillary pressure curve (P_c-curve) for the coarse sand was obtained by use of a centrifuge. Leverett's J-function was used to scale the capillary pressure curve for the coarse sand to the corresponding Pc-curve for the fine sand. Relative permeability functions were found in the literature for sand with permeability 7.4 μm^2 and porosity 0.38 (Alhanai, 1990). The Pc-curve used by Alhanai was in good agreement with our measured data, when scaled with Leverett's J-function.

The sand packing was carried out sequentially by adding a small volume of sand (25 *ml*) in-between manual compaction. A rubber membrane was placed on top of the sand-filled model and the model was closed with an aluminium lid. By injecting oil between the rubber membrane and the lid a pressure was applied on the top of the sandpack. A potential compaction of the sand would result in a decrease in the applied pressure; but such a decrease in pressure was not observed throughout the experiments.

A nuclear imaging technique was used to measure 2D in-situ brine saturation distributions during flooding (Lien, 1987; Graue, 1988). ^{22}Na in the form of *NaCl* was used to label the brine phase, in a

concentration of 44.4 GBq/m^3. A Germanium detector, with 2.0 *keV* energy resolution, collimated to effectively cover 1.5 *cm* x 1.5 *cm*, measured the radioactivity and hence radioactive brine saturation.

The measurement grid, shown in Figure 1, consisted of 17 points horizontally, i.e. one point every 1.5 *cm* except within 3 *cm* from the ends, and 6 point vertically, one point every 1.5 *cm*, except within 0.5 *cm* from top and bottom. Counting time at each point was 3 *min*, which gave a total sampling time for one full saturation distribution of 5 *h*, corresponding to 0.05 *PV* injected brine.

The model was conveniently defined as consisting of three zones. Referring to Figure 1; Zone I was the high permeable sand on the left; Zone II was the central crossbed consisting of low permeable sand; Zone III was the rightmost high permeable sand. Saturation developments are shown in two dimensional saturation maps and as average brine saturation in each zone as function of injected porevolume.

Results and Discussion

Experimental schedule and saturation history are tabulated in Table 3, note that the residual saturations after oilfloods are listed as initial conditions for the subsequent waterfloods. In the following the experiments are reported in the order they were carried out. All the waterfloods displaced Lamp oil and were performed at a rate of 3 *ml/h*, corresponding to a water front velocity of approximately 0.26 *cm/h* (0.2 *ft/day*). Fluid properties are listed in Table 1.

Brine-brine displacement. The model, initially saturated with non-radioactive brine, was flooded with 0.85 *PV* of radioactive brine, at a rate of 3 *ml/h*. The rate was then increased to 50 *ml/h* and another 1.65 *PV* of radioactive brine was injected. Comparing effluent data and in-situ saturation measurements showed good agreement, see Figure 2, thus indicating true saturation information. The density of the radioactive and non-radioactive brine was the same.

Refraction across the boundary between the high and low permeable media (Roti and Dawe, 1994) was detected in this miscible displacement, see Figure 3. Radioactive brine initially showed a uniformly vertical distribution entering Zone I, but when encountering the crosslayer, Zone II, a refracted saturation field was observed. Energy considerations imply that the flow will minimise the distance flooding in the low permeable crossbed, thus causing refraction at the permeability contrast, observed as a change in flow direction.

First oilflood. During the first oilflood the capillary number was sequentially increased by subsequently increasing flow rates and oil viscosity. In Table 2 the average brine saturations for the whole model are tabulated. The corresponding in-situ brine saturation development is shown in Figure 5.

Initially oil entered the upper part of Zone I due to gravity; gravity was influential throughout the oilflood causing the model to drain Zone I and later Zone III from top to bottom. An effective drainage of Zone II occurred only after the oil injection rate was increased substantially. The threshold pressure for entering Zone II was not reached for low injection rates, in spite of a large decrease in brine saturation in Zone I. This indicates that the viscous force establish a capillary pressure in between the two thresholds pressures for the well sorted sands, hence creating a significant saturation difference in the two sands.

For the continued more viscous dominated oilflood the recovery mechanism was different due to override of the gravity forces and reduced importance of the capillary forces. The viscous force caused the lower part of the central Zone II to be oilflooded, and at a later stage started to oilflood the lower part of the outlet sand, Zone III. The saturation distribution when 1.04 PV and 3.09 PV had been injected, Figure 5, shows stagnant brine in the upper part of the central crosslayer, even at high flow rates. This was probably due to a combination of low relative permeability to brine in the outlet sand, high relative permeability to oil in the lower part of Zone II and downward oil refraction. A reversal of flow direction redistributed the stagnant brine to a more uniform saturation within each zone; further brine production was however not observed.

First waterflood (from left). After the first waterflood the average brine saturation based on in-situ saturation profiles was 0.84 and agreed with the corresponding value from effluent data, 0.82, see also Figure 2. Based on effluent information only the high oil recovery at breakthrough could indicate a

homogeneous reservoir. However, by examining the local in-situ saturation, see Figure 4 and Figure 6, it is evident that the heterogeneity seriously impacts the local recovery.

The saturation distribution showed that the injected brine fingered through the lower part of Zone I, due to gravity and geometry, and imbibed into the central Zone II. A resulting low relative permeability to oil in Zone II reduced the oil recovery rate from Zone I. This resulted in a higher oil production rate from Zone III compared to Zone I. The development was amplified by the accumulation of brine in Zone III due to the capillary outlet end effect. The saturation distributions revealed that the oil was recovered from the lower part due to both gravity and the heterogeneous configuration, see Figure 6.

For all the water displacement experiments the outlet end effect was pronounced, and was the main reason for the late water breakthrough. The general appearance where the central crosslayer was imbibed before the inlet and outlet zones is however not disturbed by the outlet end effect.

Second oilflood. The average residual brine saturation after the second oilflood calculated from effluent data was 0.26, which agrees with the average in-situ measured brine saturation of 0.28. Table 2 shows the applied capillary numbers and the resulting average brine saturations. Table 2 also shows that a higher capillary number than used during the first oilflood, had to be applied in the second oilflood to obtain a comparable low residual brine saturation. This is due to the different initial phase distributions for the floods. Even after the high rate oil flood, with high viscous oil, Zone II maintained a higher brine saturation than the surrounding low capillary sand, see Figure 7.

Second waterflood (from right). In this waterflood the brine was injected from the right hand side, see Figure 8. The flood was stopped at water breakthrough and the model was in a no flow situation for 100 *h*; the injection was continued for an additional 0.66 *PV* of brine, at the same injection rate, see Table 3 and Figure 4.

Incipient in the brine injection the gravity caused brine to enter Zone III in the lower part, see Figure 8. Zone II was therefore later contacted by the waterfront, thus exhibiting brine imbibition of Zone II at a later stage compared to the first waterflood. This caused high recovery rate early in the waterflood. Besides this effect the influence of the low permeable crossbed appeared to be independent of the flow direction, i.e. similar for 30° and 150° dip angles.

Capillary imbibition during the no flow period in the second waterflood established a capillary equilibrium, hence a more even saturation distribution within each sand was obtained. This in turn resulted in a lower residual oil saturation after the continued waterflood.

Third oilflood. The third oilflood was performed using high viscous mineral oil, Marcol 172, at a flow rate of 360 *ml/h*, corresponding to a capillary number of $25.6\ 10^{-4}$. The resulting average residual brine saturation was 0.20, compared to 0.15 after the second oilflood. Impact of the lower capillary number is found in Figure 9 and Table 3 showing a significant higher water saturation in Zone II.

Third waterflood (from left). This experiment repeated the first waterflood to test the reproducibility. The third waterflood was initiated at a lower initial brine saturation than the first waterflood. As a result of the difference in mobile oil a time shift can be observed in the saturation development, which results in a slightly delayed waterflood in Zone III, see Figure 4. Comparing Figure 6 and Figure 10 indicates an overall good reproducibility.

Fourth oilflood. A total of 11 *PV* Marcol 172 was injected at a rate of 150 *ml/h* ($Ca=10.6\ 10^{-4}$) during the fourth oilflood. Both the average residual saturation, $S_w=0.20$, and the brine saturation within each zone was similar to the previous oilflood at twice the capillary number.

Simulations

A full field commercial simulator, ECLIPSE, was used to numerically simulate the waterfloods. ECLIPSE uses a five point difference scheme to solve the flow and pressure equations, for two dimensional grids. This means that flow is only calculated through the four faces on a square lattice; any dipping layer is consequently modelled as a stair on a regular lattice. The simulation model was not scaled with regard to size, pressure or physical data for the two sands. Further simulation details can be found in Børresen and Graue 1996.

Incipient imbibition of Zone II was fairly accurately predicted for the first and the third waterflood, see Figure 11. The brine saturation in Zone I increased too fast in the simulations which later lead to

an underestimation of waterflooding in Zone II. The saturation development observed experimentally, with rapid increase of brine saturation in Zone II, might be difficult for the simulator to handle due to the difference in saturation between the high and the low permeable media. Generally saturation gradients are smeared out by numerical diffusion. The simulator is hence expected to underestimate the increase in brine saturation in Zone II while Zone I and/or Zone III are expected to attain a slightly higher brine saturation than experimentally observed.

Simulation of the second waterflood underestimated the effects of gravity, and this caused a serious underestimation of brine saturation in the inlet sand, Zone III. Further, in the simulations, Zone II was contacted early by the waterfront and rapid imbibition of this zone occurred. This lead to temporarily bypassed oil in Zone III, which was not recorded experimentally.

A grid sensitivity study was performed and was used to define the required grid resolution used in the numerical simulator. Further, different relative permeability curves as input for the simulator were tested and found uninfluential on the simulations of the low rate waterfloods.

The simulations show that care has to be taken when interpreting numerical results without information on local saturation distribution. Simulations captured the general saturation development in the experiments but missed the finer details, see Figure 11. The simulations accurately predicted a higher brine saturation in the outlet sand, compared to the inlet sand, as experimentally observed. The water breakthrough was correctly predicted in the simulations.

Conclusions

A two dimensional nuclear tracer imaging technique used to study water- and oilfloods in the heterogeneous, cross bedded, reservoir model showed that a permeability contrast of a factor of two distort the local saturation development.

During the low rate oilfloods a non-uniform immobile water saturation was obtained; the central low permeable sand had a substantially higher residual water saturation. Even at high capillary number oilfloods, stagnant brine was observed at the top of Zone II.

The low permeable crossbed reached a high brine saturation at an early stage of the waterfloods. As the central low permeable zone approached residual oil saturation the outlet sand was flooded and attained temporarily a higher brine saturation than the inlet sand, indicating temporally oil trapping in Zone I. However, the inlet- and outlet sands had similar residual oil saturations at the termination of the waterfloods, hence no permanent trapped oil was observed.

In this water wet sand only small changes in the local brine saturation was observed after breakthrough.

The commercial simulator ECLIPSE was found to give a qualitatively correct description of the local saturation development experimentally observed. Numerical diffusion probably induced an unrealistic high waterfront velocity and hence the finer details in the experimentally observed local saturation development could not be matched.

References

Ahmed, G., Castanier, L. M. and Brigham, W. E.: "An Experimental Study of Water flooding From a Two-Dimensional Layered Sand Model", SPE Reservoir Engineering, February (1988).

Alhanai, Waddah: "Multi-phase flow in heterogeneous porous media: Theoretical and experimental results for nodular systems", PhD Thèse L'Université de Bordeaux I (1991, in English).

Bertin, H., Graue, A., and Eilertsen, T.: "Two Dimensional Imaging of Viscous and Capillary Effects in a Dipping Stratified Heterogeneous Media", Proceedings International Symposium of the SCA, Stavanger Norway, September 13-14 (1994), 141-148.

Bertin, H. and Quintard, M.: "Two-Phase Flow in Heterogeneous Porous Media II: Laboratory Experiments for Flow Parallel to a Stratified System", Transport in Porous Media 5 (1990), pp. 543-590.

Børresen, K.A. and Graue, A.: "Numerical Simulations and 2D Imaging Experience of Fluid Flow in a Dipping Crossbedded Reservoir Model" to be published at 71th SPE ATCE, Denver, October 6-9 (1996), SPE 36731.

Chang, J. and Yortsos, Y. C.: "Effect of Capillary Heterogeneity on Bucley-Leverett Displacement", SPE Reservoir Engineering, May (1992), SPE 18798.

Chaouche, M., Rakotomalala, N, Salin, D., Xu, B., and Yortsos, Y.C.: "Capillary effects in drainage in heterogeneous porous media: continuum modelling, experiments and pore network simulations", Chem. Eng. Sci., Vol. 49, No. 15 (1994), pp. 2447-2466.

Graue, A., Kolltveit, K., and Lien, J.R.: "Imaging Fluid Saturation Development in Long Coreflood Displacements", SPE California Regional Meeting, March 23-25 (1988), SPE 17438. Printed in SPEFE December 1990.

Graue, Arne: "Imaging the Effects of Capillary Heterogeneities on Local Saturation Development in Long core Floods", SPE Latin American Petroleum Engineering Conference, Rio de Janeiro, October 14-19 (1990) SPE 21101. Printed in SPEDC, March (1994).

Graue, A. and Pedersen, E.: "Two Dimensional Imaging of Fluid Flow in a Large Slab of Heterogeneous, Cross Bedded Sandstone", Proc. 8th European Symp. on Improved Oil Recovery, Vienna, Austria, May 15-17, (1995).

Hartkamp-Baker, C.A.: "Permeability heterogeneity in cross-bedded sandstones Impact on water/oil displacements in fluvial reservoirs", PhD thesis, Tech. Univ. Delft, Netherlands (1993).

Honarpour, M.M., Cullick, A.S., Saad, N., and Huphreys, N.V.: "Effect of Rock Heterogeneity on Relative Permeability: Implications for Scaleup", JPT Nov. (1995), pp 980-986, SPE 29311.

Laribi, S., Bertin, H., Quintard, M., "Two-phase calculations and comparative flow experiments through heterogeneous orthogonal stratified systems", J. of Petroleum Science and Engineering 12, (1995) 183-199.

Lien, J.R., and Kolltveit, K.: "A Nuclear Technique for Studying Multiphase Flow in a Porous Medium at Oil Reservoir Conditions", Nuclear Instruments and Methods in Physical Research, A 271, (1987) 693-700.

McDougall, S.R., and Sorbie, K.S.: "The Combined Effect of Capillary and Viscous Forces on Waterflood Displacements Efficiency in Finely Laminated Porous Media", 68th SPE ATCE, Houston, October 3-6 (1993), SPE 26659.

Ringrose, P.S., Sorbie, K.S., Corbet, P.W.M., Jensen, J.L.: "Immiscible flow behaviour in laminated and cross-bedded sandstone", J. of Petroleum Science and Engineering (1993), 9, pp. 103-124.

Roti, Ø, and Dawe R. A.: "Modelling Fluid Flow in Cross-bedded Sections", Trans. in Porous Media 12, pp. 143-159 (1993).

Sorbie, K. S., Wat, R. M. S. and Rowe, T. C.: "Oil Displacement Experiments in Heterogeneous Cores: Analysis of Recovery Mechanisms", 62th SPE ATCE, Dallas, September 27-30 (1987), SPE 16706.

Wright, R. J. and Dawe, R. A.: "Fluid Displacement Efficiency in Layered Porous Media Mobility Ration Influence", Revue de L'Institue Francais du Pètrole, Vol. 38, No. 4 (1983).

Fluid	Density $[kg/m^3]$	Viscosity $[mPa\,s]$	Surface tension brine/oil $[mN/m]$
Brine	1030	1.07	-
Lamp oil	740	1.43	67.08
Marcol 82	850	25	37.26
Marcol 172	850	72	56.20

Table 1 *Fluid properties.*

		Initial	Lamp Oil		Marcol 82				Marcol 172
OF1	Rate $[ml/h]$		3	50		50	200		100
	$Ca\,10^{-4}$		0.006	0.13		1.86	7.46		7.12
	S_w	1.00	0.70	0.53		0.31	0.22		0.22
OF2	Rate $[ml/h]$				3	30	120	360	500
	$Ca\,10^{-4}$				0.11	1.12	4.47	13.42	35.59
	S_w	0.83			0.79	0.73	0.70	0.26	0.15

Table 2 *First and second oilflood (OF): Residual brine saturation, S_w, after each increase in capillary number, Ca.*

	Initial Brine Saturation				Final Brine Saturation				Water	Injected
	Z I	Z II	Z III	Av	Z I	Z II	Z III	Av	B.T.	W.$[PV]$
WF 1	0.20	0.34	0.21	0.24	0.84	0.87	0.83	0.85	0.71	1.20
WF 2	0.14	0.17	0.15	0.15	0.79	0.82	0.75	0.78	0.66	0.66
WF 2					0.88	0.90	0.87	0.88		0.62
WF 3	0.18	0.28	0.17	0.20	0.85	0.87	0.83	0.85	0.67	1.27
4th oilflood	0.18	0.27	0.17	0.20						

Table 3 *All waterfloods (WF) were performed at brine injection rate of 3 ml/h. The table shows initial and final brine saturation for each Zone (ZI, ZII, and ZIII), the average measured in-situ brine saturation (Av), and water breakthrough (B.T.).*

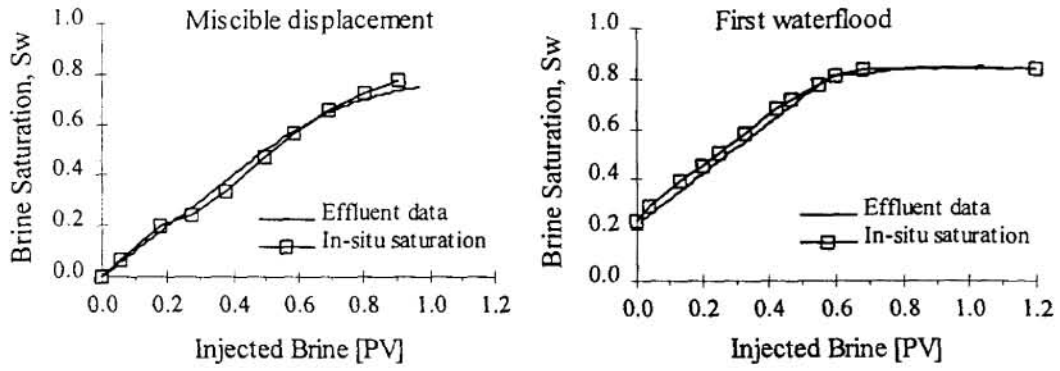

Figure 2 *Production data based on in-situ saturation and effluent data during miscible and immiscible displacements.*

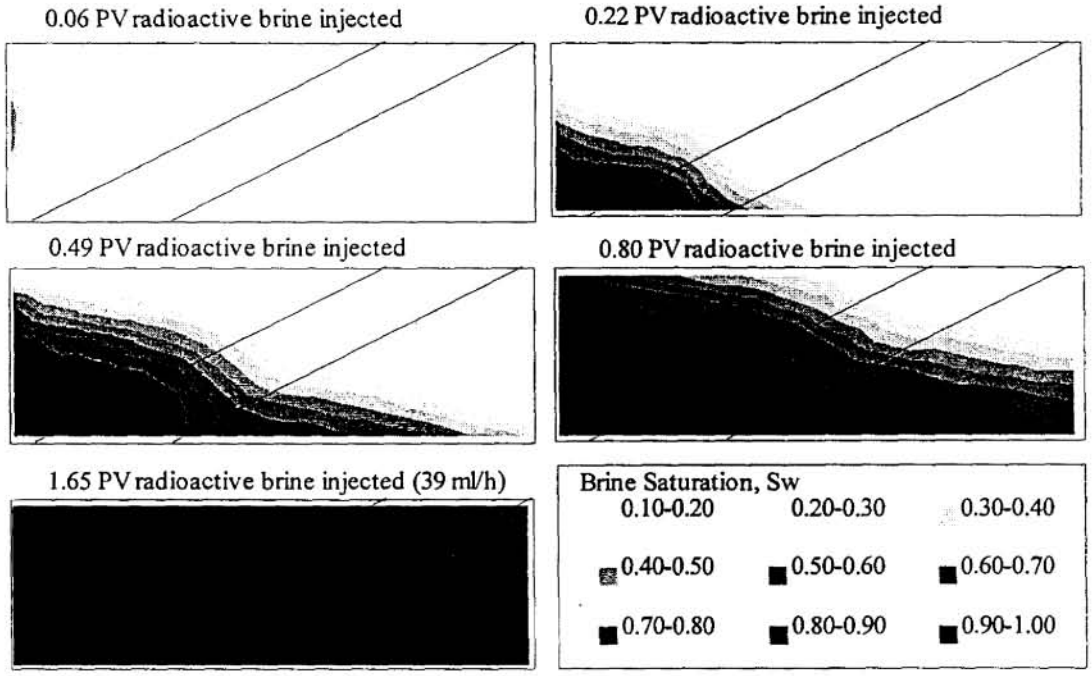

Figure 3 *Radioactive brine displacing non-radioactive brine in miscible displacement.*

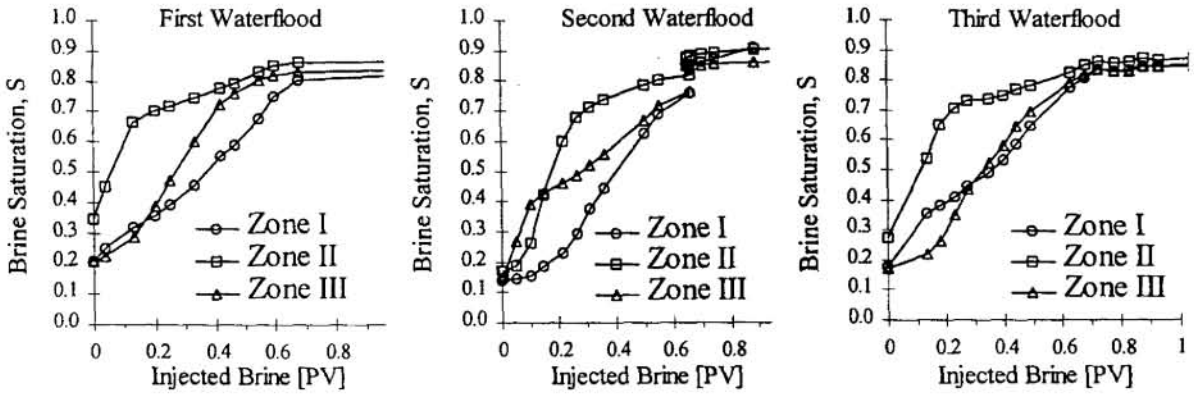

Figure 4 *Average brine saturation development for the different zones during the waterfloods.*

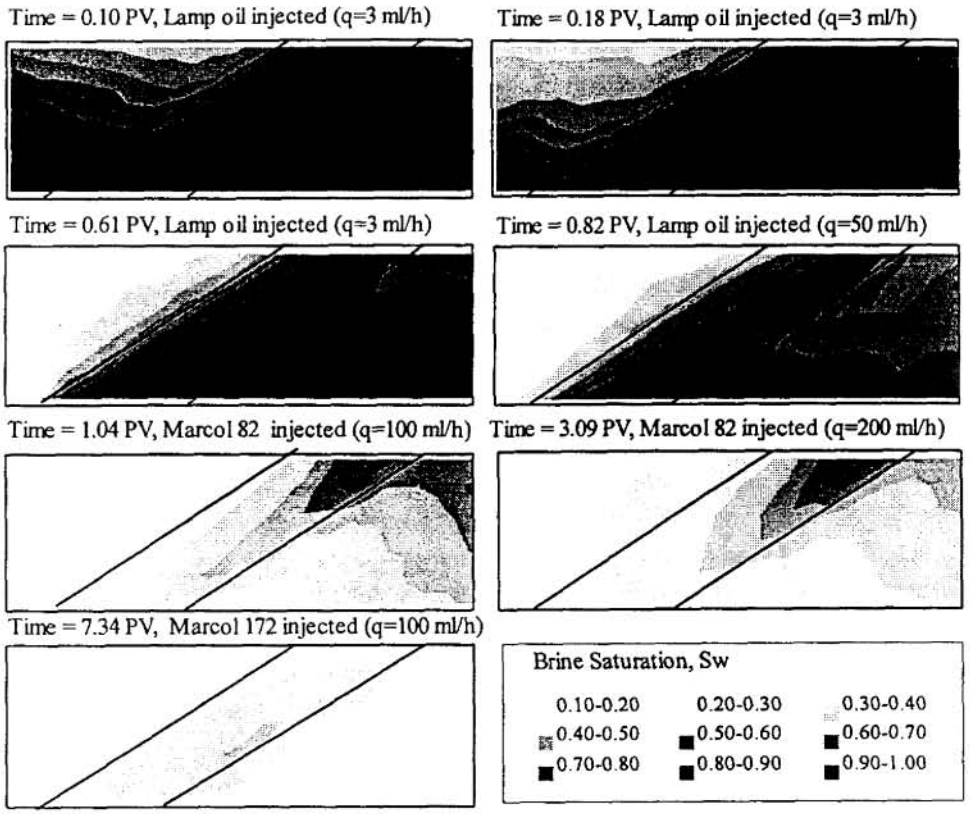

Figure 5 *First oilflood. Oil viscosities and oil injection rates was gradually increased.*

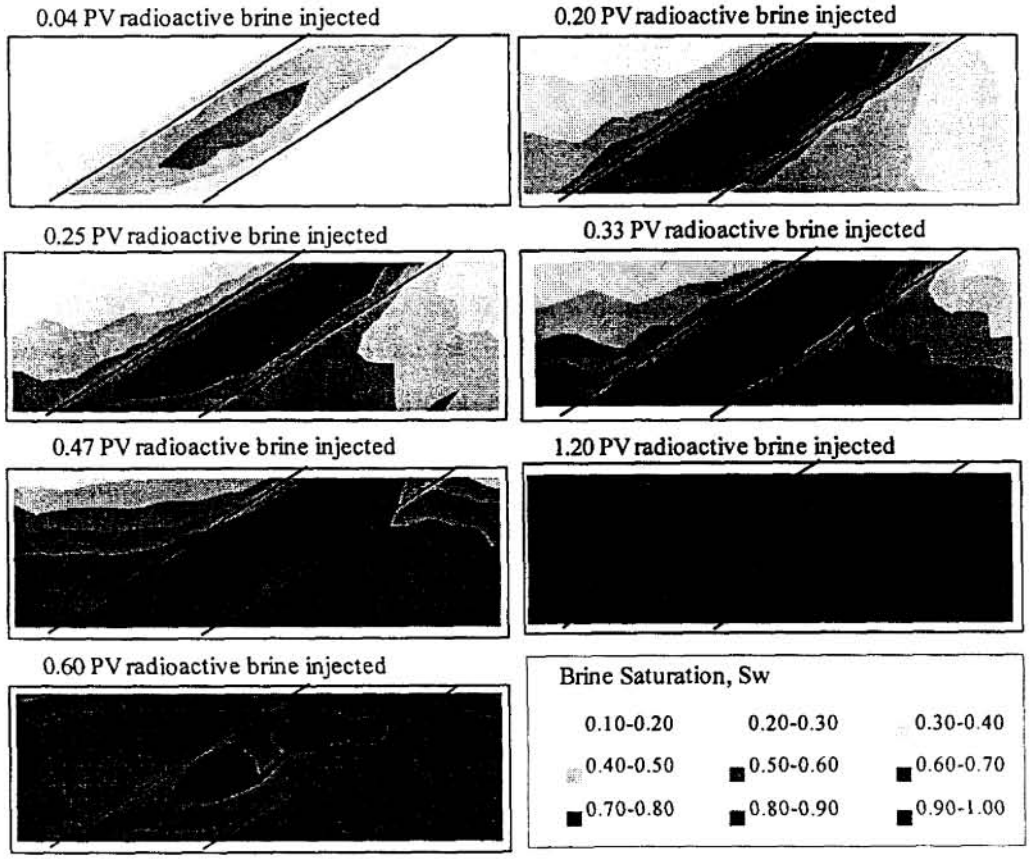

Figure 6 *First waterflood. Brine was injected from left in the figures.*

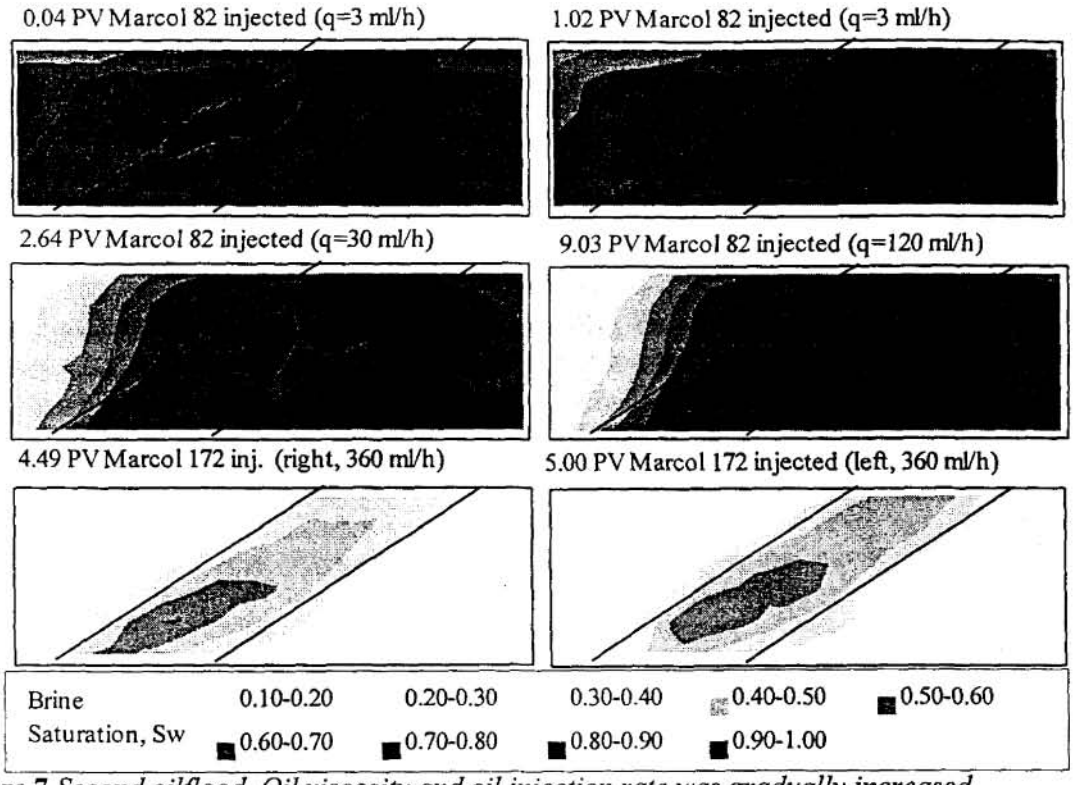

Figure 7 *Second oilflood. Oil viscosity and oil injection rate was gradually increased.*

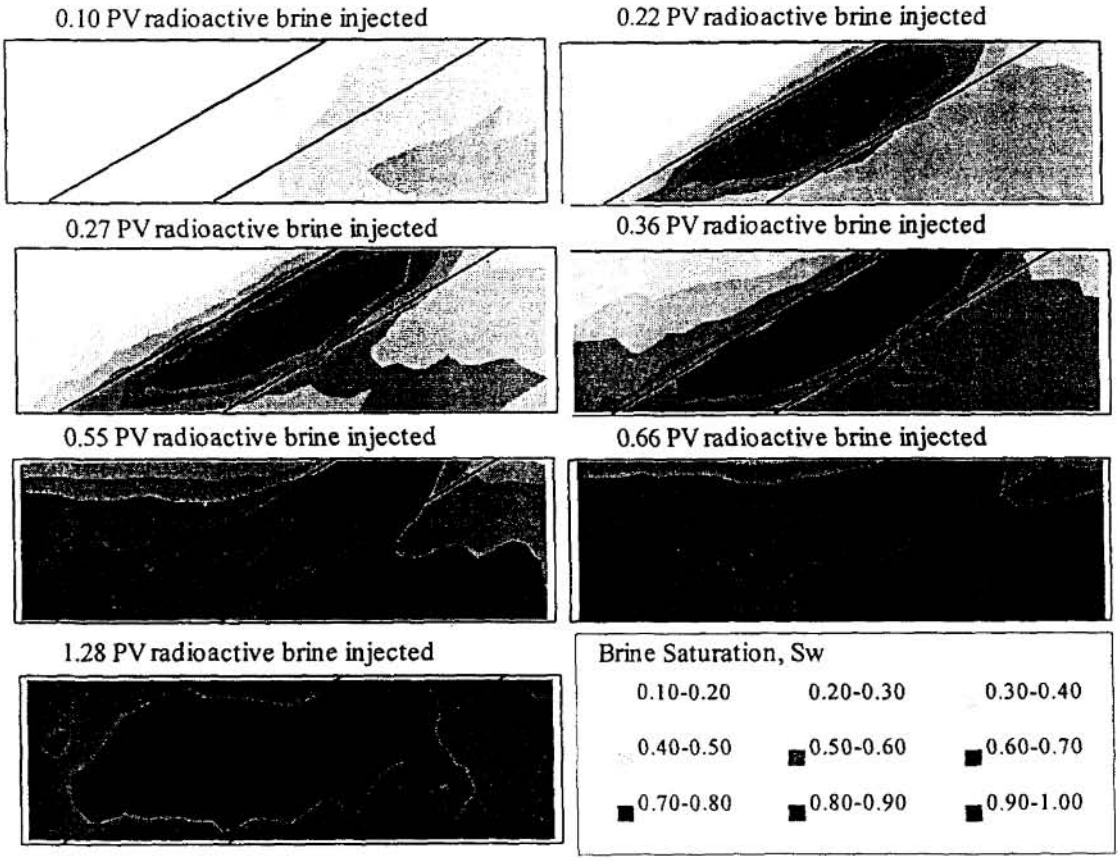

Figure 8 *Second waterflood. Brine was injected from right in the figures.*

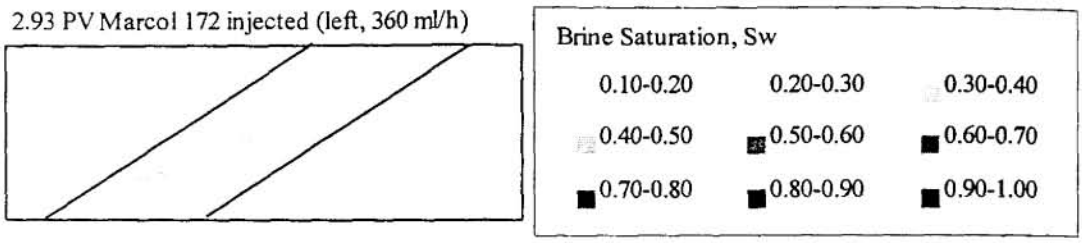

Figure 9 *Third oilflood, residual brine saturation.*

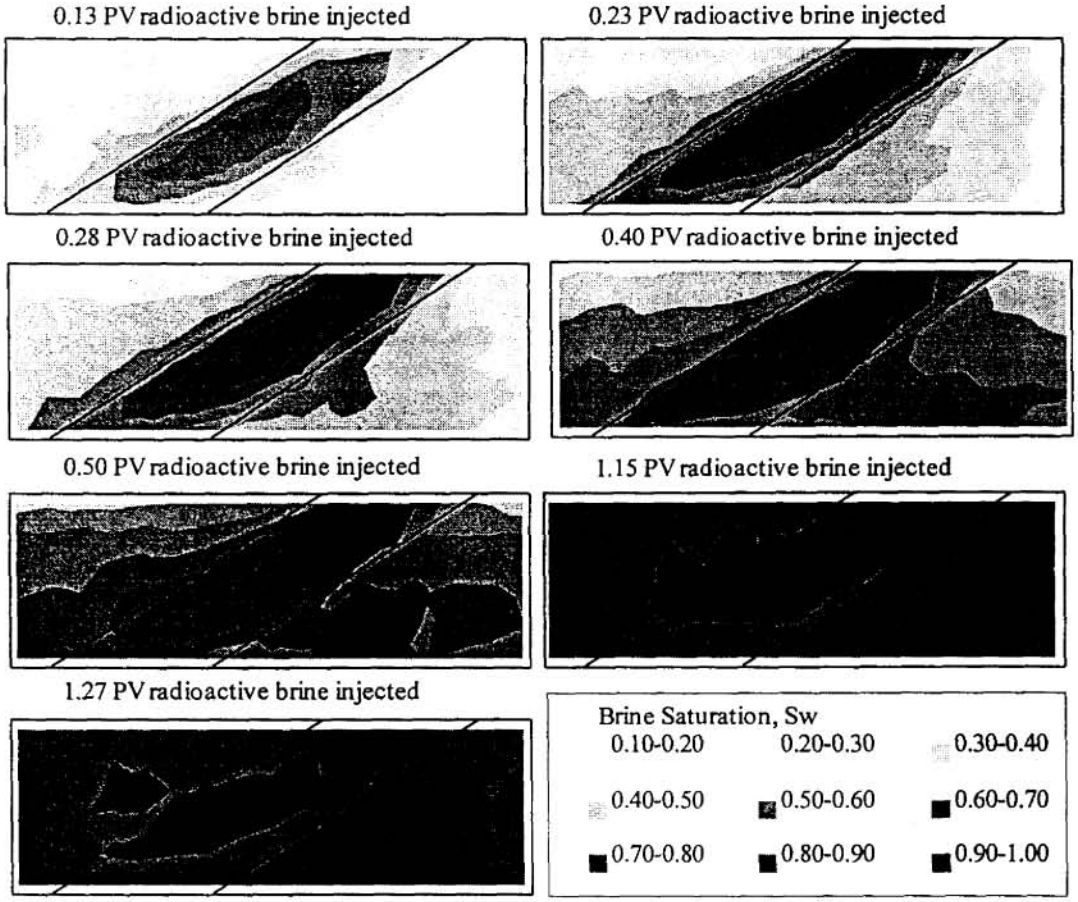

Figure 10 *Third waterflood. The brine was injected from left in the figures.*

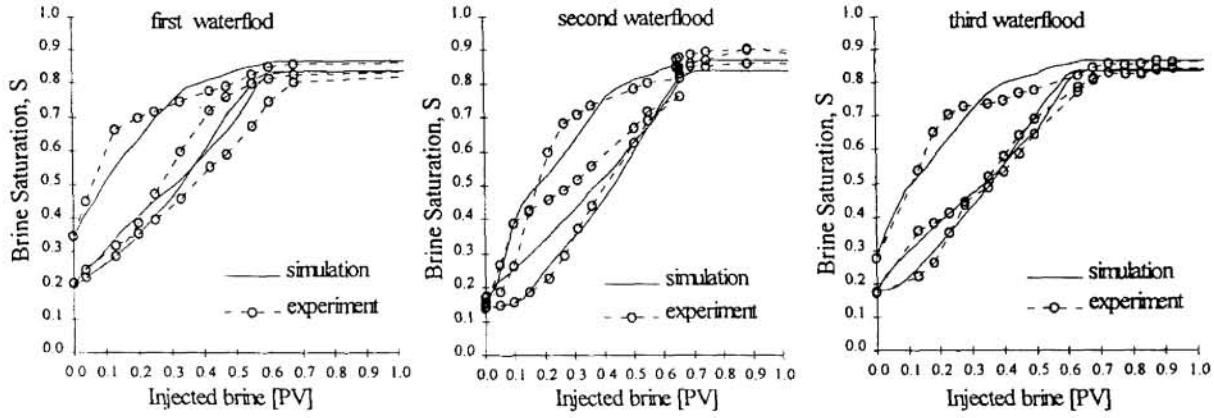

Figure 11 *Comparison of experiments and simulations for the three waterfloods.*